Check for updates

Interactions, electronic and optical properties of nanographene–peptide complexes: a theoretical study†

Ruby Srivastava 🆔 *

We studied the interaction of planar phenylalanine (**phe**), tryptophan (**try**), tyrosine (**tyr**); amide asparagine (**asn**) and glutamine (**gln**); arginine (**arg**) side-chains, charged histidine (**his-c**) and charged lysine (**lys-c**) side-chains on a nanographene (**g**) surface by Density Functional theory (DFT) and Time Dependent Density Functional Theory (TDDFT). The occupied number of states by the system at each energy level and relative contribution of a particular atom/orbital has been studied by Density of States (DOS) and Partial Density of States (PDOS) respectively. Atom-in Molecules (AIM) analysis and non-covalent interaction (NCI) PLOT are used to study the interactions in these complexes. The absorption spectra and HOMO–LUMO (HL) gaps are quantitatively analysed to study the correlation between the optical properties of the studied complexes. The HL gap of peptides is larger than the HL gap of graphene–peptide complexes, indicating strong interactions. All the peptides interact from the above the nanographene surfaces. **garg**, **glys-c**, **gtry** and **gtyr** complexes have smaller bond distance as compared to **gasn**, **ggln**, **ghis-c** and **gphe** complexes. AIM analysis and (NCI) PLOT showed noncovalent interactions for these complexes. TDDFT calculations indicated the applicability of these complexes as biosensors.

1. Introduction

Graphene, a two-dimensional (2D) sp^2-hybridized single atomic layer of carbon material, chemically bonded with hexagonal symmetry, has been used widely with many potential applications[1,2] for nanobio-medicine and nanobio-sensing.[3–6] Due to its optoelectronic, absorption, sensing and catalytic properties, graphene plays a key role in the development of photovoltaics, optical switches, actuators, photodetectors, photo-catalysts, photo modulators, photo-thermal therapy and bioimaging.[1c] Graphene has also been widely used as active or scaffold materials,[7,8] electronic devices,[9–11] energy storage systems,[12,13] energy conversion devices,[14,15] and bio/chemical sensors.[16] It has been seen in recent years that a variety of short peptide probes have been identified as biomarkers for many diseases. The noncovalent graphene–peptide based biosensors are used with excellent diagnostic function, due to large 2D aromatic surface of graphene, immobilization of biomolecules and its π–π stacking interaction. Thus it is necessary to find out the specific adsorption configurations of biological molecules (proteins or peptides) to ensure the availability of one section of the biomolecule to be solvent exposed, and simultaneously, the strong binding of the other section of the biomolecule to the

graphene surface. π–π interactions (or stacking) of the aromatic functionalities have been very important interactions between different peptide side chains, between side chain and backbone, and between peptide side chain and graphene surfaces.[17–23] Usually graphene has a planar aromatic dominant structure and it binds with peptide side chains with aromatic or amide groups.[17,22] Previous reports indicated strong binding affinity between a graphene surface and peptide side chains with planar groups.[24–27] π–π interactions plays an important role in the adsorption behavior and peptide orientation preference on a graphene surface, so it is very important to study its interactions. It has been observed that enzyme immobilization on graphene or graphene oxide occurs due to weak interactions, which included hydrophobic, electrostatic, and π–π stacking interactions. Studies conducted for short-chain peptides bonded to graphene indicated that small peptides assemble prefer to the edge or planar surface of graphene *via* electrostatic or π–π interactions.[28–31] As peptides has simple structures, it is usually easy to study graphene–peptide interactions. The conformational changes can also predicted by both experimental[32] and theoretical means.[33] In a previous study of graphene and carbon nanotubes interaction with phenylalanine (**Phe**), histidine (**His**), tyrosine (**Tyr**), and tryptophan (**Trp**) molecules, it was observed that the aromatic rings of these amino acids prefer parallel orientation with the plane of graphene and CNTs through π–π interactions.[33] Based on the experimental studies,[16] we have selected eight arginine (**arg**), asparagine (**asn**), glutamine (**gln**), cationic-histidine (**his-c**),

CSIR-Centre for Cellular and Molecular Biology, Hyderabad, India. E-mail: amitruby1@gmail.com; ruby@ccmb.res.in

cationic-lysine (**lys-c**), phenylalanine (**phe**), tryptophan (**try**), tyrosine (**tyr**) peptides and a nanographene (**g**) surface to study the electronic, optical properties and interaction of graphene–arginine (**garg**), graphene–asparagine (**gasn**), graphene–glutamine (**ggln**), graphene–cationic histidine (**ghis-c**), graphene–cationic lysine (**glys-c**), graphene–phenylalanine (**gphe**), graphene–tryptophan (**gtry**) and graphene–tyrosine (**gtyr**) complexes by DFT and TDDFT methods.

2. Calculation method

Conformational search has been carried out on all amino acids, (rotation about each single bond) by G09 (ref. 34) software using B3LYP[35a]/6-31G* method and based on lower energy conformations the final structure has been reoptimized using two different DFT methods. The energy values of the optimized peptide with three different approaches (a)B3LYP[35a]/6-31 G*, (b) M06 (ref. 35b)/6- 31G* and (c) B3LYP-D2 (ref. 35c)/6-31G* is given in ESI Table 1.† Finally the lowest energies obtained by B3LYP-D2/6-31G(d,p) method is used for all calculations. B3LYP-D2 functional is selected to include the dispersion correction energy term which is relatively simple function of interatomic distances and contain adjustable parameters to fit the conformational and interaction energies.

Initial configuration of nanographene is built by Avogadro package[36] with UFF force field. The nanographene sheet has a planar neutral singlet structure with 72 carbon atoms. To maintain the consistency of results, the structure of

nanographene is reoptimized again with B3LYP-D2/6-31G* method. Vibrational frequency analysis has been carried out for all complexes to confirm the stability of these complexes and it was found that there is no negative frequency for the reported complexes. Various initial spatial (guessed) arrangements of amino acid residue above the nanographene has been made and optimized with B3LYP-D2/6-31G* method and finally the structures with lowest energy minima was reported in Fig. 1. Again vibrational frequency analysis has been carried out for the stability of these nanographene–peptide complexes and no negative frequency has been found for all the reported complexes.

Gaussview[37] is used for visualization of structures and NCI-PLOT figures. All the calculations have been carried out with self-consistent reaction field (SCRF) theory with polarizable continuum method (PCM).[38] The dielectric constant was chosen as the standard value for water ($\varepsilon = 78.39$). TDDFT calculations are also carried out with the same level of B3LYP-D2/6-31G* method, as in terms of reliability also, state-specific dispersion correction is desired, in which the electron redistribution induced by electronic excitation should be reflected in the calculations.

First-principles calculations are performed on the optimized geometries of complexes in solvent (water) using the density functional theory (DFT) approach implemented in SIESTA[39] (Spanish Initiative for the Electronic Simulations with Thousands of Atoms) 4.1.b4 program package. In addition, the van der Waals density functional (vdW-DF) as proposed by Dion
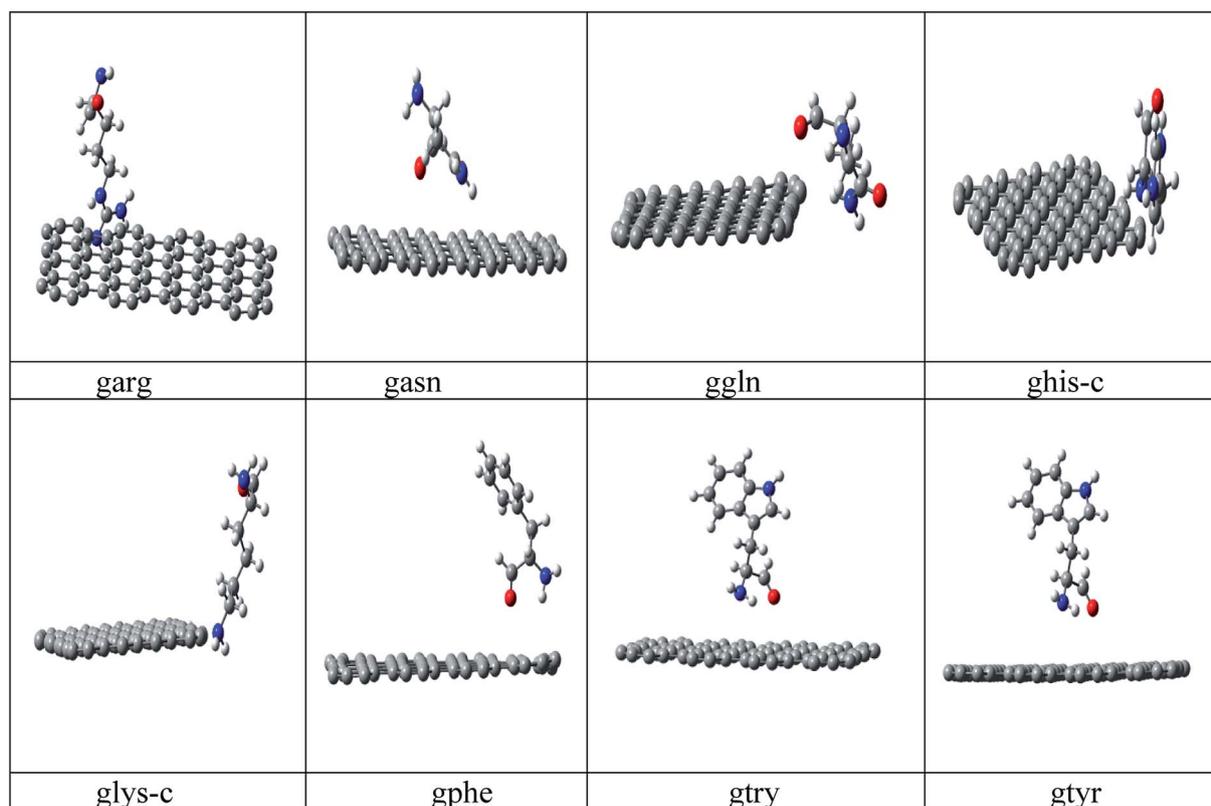

Fig. 1 Optimized structures of the studied nanographene–peptide Complexes in aqueous medium by DFT method.

et al.[40] is used to calculate the adsorption energies for these models. The exchange and correction terms are described using generalized gradient approximation (GGA) in the scheme of the Perdew–Burke–Ernzerhof (PBE) functional. Double-ς basis set plus polarization function[41] is used for all the calculations. Lattice constant 1 Å, Monkhorst pack of $2 \times 2 \times 0.5$ *k*-point mesh for Brillouin zone integration, cut-off 300 Ry and Gaussian smearing of 0.10 eV are used for the Density of States (DOS) and partial density of states (PDOS) calculations (Fig. 2).

The properties of bond critical points (BCPs) are performed by AIM analysis with AIM 2000 package.[42,43] Two of its charge density-based topological descriptors, *i.e.* bond path (bp) and the presence of (3, −1) bond critical point (bcp) between interacting atomic basins have proved very useful in inferring the presence of a chemical bonding in these chemical systems, which has been used here for the calculations.

2.1. Atoms-in-molecules analysis

The Laplacian of electron density $\nabla^2 \rho(r)$ at the bond critical point is given by the local expression of virial theorem as,[42]

$$\frac{1}{4}\nabla^2 \rho(r) = 2G(r) + V(r) \tag{1}$$

In which $G(r)$ and $V(r)$ are kinetic and potential energy densities respectively. A negative value of $\nabla^2 \rho(r)$ show excess potential energy at BCP, which is the condition of all shared electron covalent interactions. A positive $\nabla^2 \rho(r)$ value shows excess kinetic energy and indicates closed shell electrostatic interaction. It also predicts the depletion of electronic charge
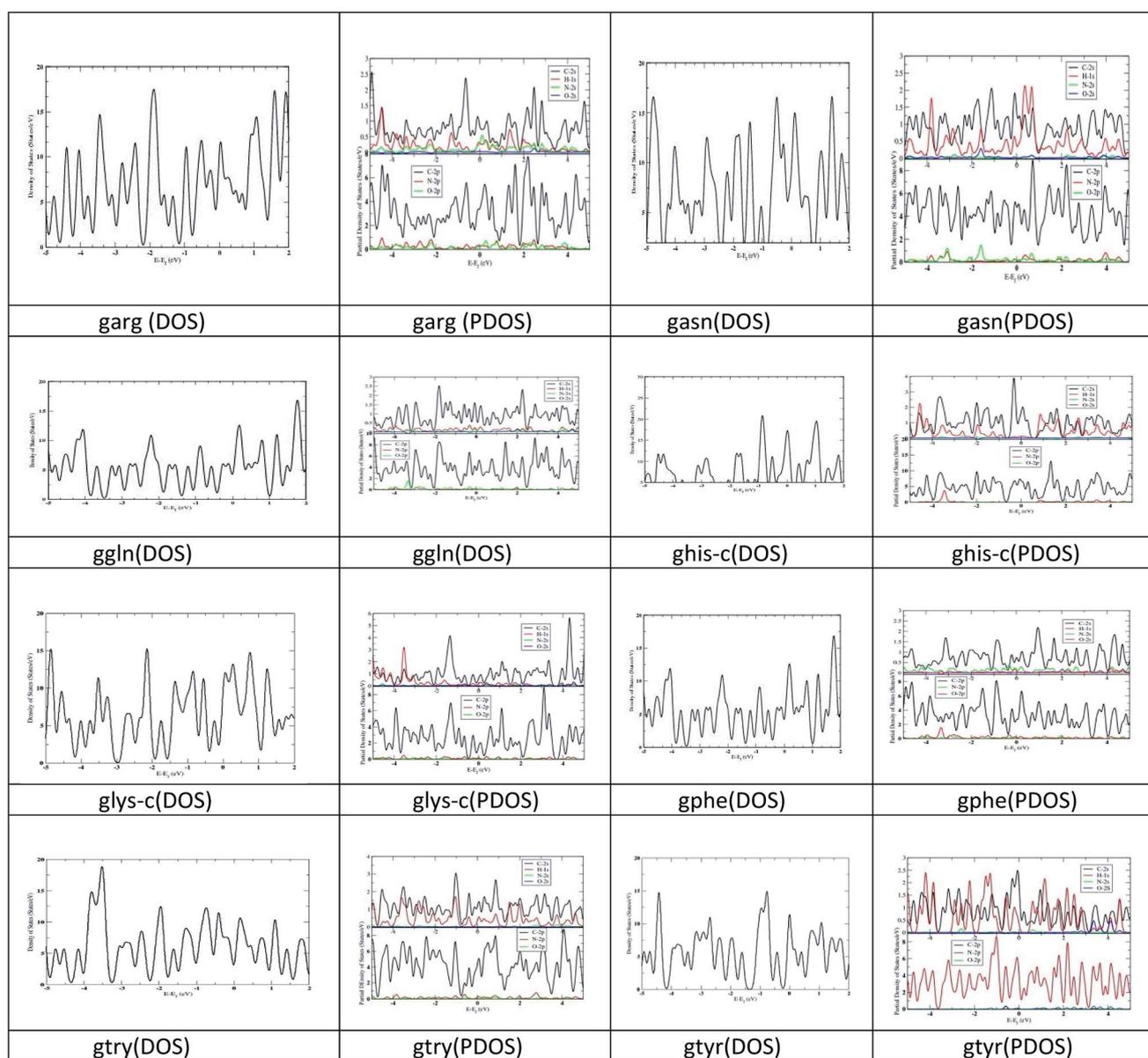

Fig. 2 Density of States (DOS) and Partial Density of States (PDOS) for the studied complexes.

Table 1 Bond distance (Å) of the interacted peptide atom (N/O) to the graphene, adsorption energy $-E_{ad}$ (B3LYP-D2, GGA(vdW)) eV, Mulliken charges of the interacted graphene (C) and peptide nitrogen(N)/oxygen (O) atom (au), difference in Mulliken charges of the two interacting atoms (Δq) (au) in aqueous medium by DFT method

| Complexes | Bond distance (Å) | $-E_{ad}$ (eV) | | Charge (C) | Charge (N/O) | Δq |
		B3LYP-D2	GGA (vdW)			
garg	2.919	11.87	11.09	0.0644	0.0001 N	0.0643
gasn	5.038	9.78	8.47	0.0563	−0.4577 O	0.4014
ggln	6.185	13.84	12.43	0.0633	0.0000 N	0.0633
ghis-c	6.152	16.61	16.07	0.0142	0.0000 N	0.0142
glys-c	3.824	21.16	20.88	0.1132	−0.4402 O	0.3270
gphe	5.543	13.70	12.97	0.0072	−0.3309 O	0.3237
gtry	4.727	13.83	13.68	−0.1427	−0.3287 O	0.1860
gtyr	4.845	13.81	12.88	0.0598	0.0001 O	0.0597

over the bond length. The electron density Hamiltonian $H(r)$ is given by the following equation

$$H(r) = G(r) + V(r) \qquad (2)$$

Koch and Popelier[43] proposed both $\nabla^2\rho(r) > 0$ and $H(r) > 0$ for weak and medium bonds; $\nabla^2\rho(r) > 0$ and $H(r) < 0$ for strong hydrogen bonds and both $\nabla^2\rho(r) < 0$ and $H(r) < 0$ for very strong hydrogen bonds.

It has been observed in recent years that because of the precise criteria, AIM analysis sometimes failed to identify weakly bound and van der Waals interactions in chemical systems.[44–48] So the Reduced Density Gradient-Non Covalent Interaction (RDG-NCI) approach is used to investigate the interactions for graphene–peptide complexes. The detail discussion regarding NCIPLOT[49] is given in results section.

3. Results and discussion[1]

3.1. Optimized geometries of nanographene and peptides

The optimized geometry of nanographene and peptides (**arg, asn, phe, gln, his-c, lys-c, try** and **tyr**) are given in ESI Fig. 1.† The HL gap, dipole moment and polarizability of these complexes are given in ESI Table 1.† The polarizability of nanographene is larger (474.22) compared to the peptide molecules. The calculated polarizabilities by our method are slightly higher than the polarizability calculated in a previous study[33] by MP2/6-31G* method, yet the polarizability trend remain same for **try** > **tyr** > **phe** > his peptides. The HL gap for nanographene (3.86 eV) is lower than the HL gap of peptide complexes. It has been observed in a previous study that the HL gap of graphene sheet varies as a function of its size and spatial variation of the electron density across the nano-graphene sheet.[2c] Peptide complexes **asn, gln, phe** and **tyr** have higher HL gaps. The trend of HL gap is **gln** > **phe** > **asn** > **tyr** > **lys-c** > **his-c** > **try** > **arg**. No correlation has been observed between polarizability and HL gap for the peptide complexes. The dipole moment of nano-graphene sheet and peptide complexes is between (0.001–5.421) debye. DOS and PDOS analysis has also been carried out for the studied structures. The DOS structures show larger band gap for **asn, gln, phe** and **tyr** and smaller band gap for nanographene

and other peptides, which has been verified by the HL gap values with DFT calculations also. See ESI Fig. 2.† PDOS figures show that the HOMO, LUMO of these nanographene–peptide complexes are solely from π electrons. See ESI Fig. 3.†

3.2. Adsorption energies and geometries

The adsorption energy of the studied complexes is calculated by the formula:

$$E_{ad} = E_{g\text{–}pep} - E_g - E_{pep} \qquad (3)$$

where $E_{g\text{–}pep}$ is the total energy of the graphene–peptide complexes, E_g is the energy of the isolated nanographene sheet and E_{pep} is the energy of an isolated peptide. The optimized structures of all the studied complexes are given in Fig. 1. The HL gap (eV), Dipole moment (debye) and polarizability of studied complexes are summarized in Table 1. It is observed that graphene has retained its planar structure while interacting with peptides. The HL gap of studied complexes is smaller than the HL gap of isolated peptide respectively, which shows strong interaction between graphene–peptide bonds. Bond distance between graphene–peptide complexes, adsorption energies $-E_{ad}$ (B3LYP-D2/6-31G*) and $-E_{ad}$(GGA-vdW), Mulliken charge of the interacted atoms and the difference between the Mulliken charge (Δq) is reported in Table 2. In all the studied complexes, graphene is interacted to the (N or O) atom of the peptides. It has been observed that **garg, glys-c, gtry** and **gtyr**

Table 2 The HL gap (eV), dipole moment (debye) and polarizability of the studied complexes in aqueous medium

Complexes	HL gap (eV)	Dipole moment (D)	Polarizability
garg	3.06	7.66	536.56
gasn	3.83	2.42	514.22
ggln	3.83	2.87	548.09
ghis-c	3.06	7.84	415.42
glys-c	4.22	2.59	444.89
gphe	3.82	2.48	526.18
gtry	3.64	2.99	552.67
gtyr	3.84	3.04	537.31

Table 3 Electron density (ρ_{BCP}, au), its Laplacian ($\nabla^2\rho_{BCP}$, au), kinetic electron energy density (G_{BCP}, au), potential electron energy density (V_{BCP}, au), total electron energy density (H_{BCP}, au) and absolute ratio (abs) of the kinetic and potential electron energy densities ($-G_{BCP}/V_{BCP}$) for the studied complexes

Complexes	ρ_{BCP}	$\nabla^2\rho_{BCP}$	G_{BCP}	V_{BCP}	H_{BCP}	$-G_{BCP}/V_{BCP}$
garg	0.18337	0.018567	0.267603	−0.265170	0.511774	1.01
gasn	0.02707	−0.03092	0.027812	−0.003100	0.024705	8.95
ggln	0.25398	0.14260	0.352636	−0.345242	0.547878	1.02
ghis-c	0.40865	−1.80950	0.423888	−0.414388	2.638276	1.02
glys-c	0.01937	−0.01611	0.014526	−0.001584	0.012941	9.17
gphe	0.00375	−0.003490	0.002761	−0.000733	0.002028	3.77
gtry	0.01165	−0.010670	0.008512	−0.002159	0.006352	3.94
gtyr	0.18173	0.027842	0.253700	−0.251543	0.475244	1.01

complexes have smaller bond distance as compared to **gasn**, **ggln**, **ghis-c** and **gphe** complexes. The adsorption energies are higher for **ghis-c** and **glys-c** complexes. The adsorption energies result for **try** > **tyr** > **phe** peptide showed similar trend as predicted in a previous study.[33] The adsorption energies with vdW corrections are lower than the adsorption energies by (B3LYP-D2/6-31G*) method. Though the trend of adsorption energies by the two methods remain same. (**glys-c** > **ghis-c** > **ggln** > **gtry** > **gtyr** > **garg** > **gasn**).

As **his-c** and **lys-c** interact to the nanographene in cationic states, the charges on the interacted atom (N/O) is zero. The aromatic rings of the peptides prefer to orient perpendicularly to the plane of the nanographene, indicating weak π–π interactions. We have not found any correlation between the polarizability and the strength of the interaction in our studied complexes. It has been observed that all peptides interact from above the nanographene surfaces.

DOS graph also reflected larger band gap for **glys-c**, **gtyr**, **gasn** and **ggln**, complexes, while the band gap is small for the other
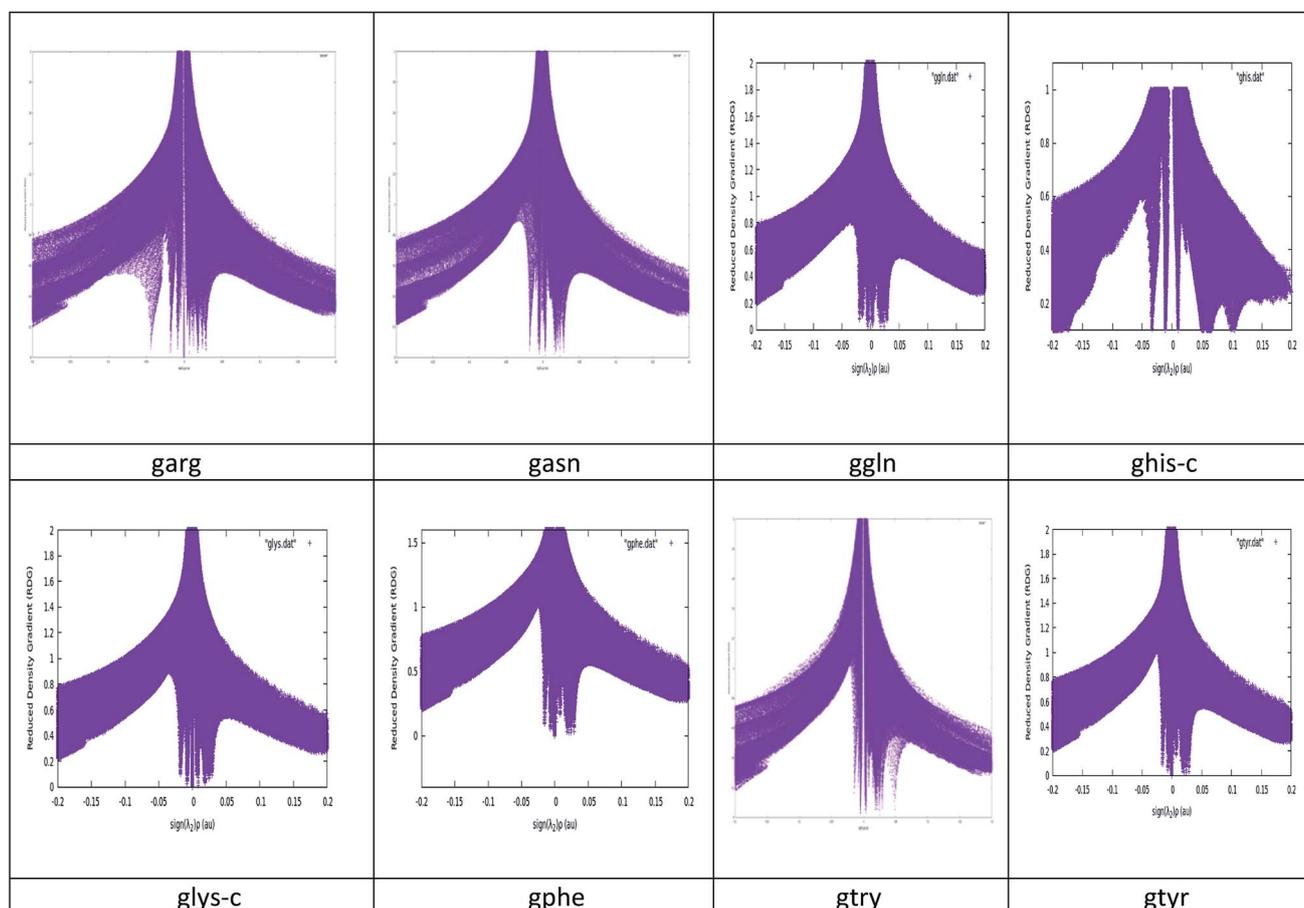

Fig. 3 Reduced density gradient (RDG) versus sign (λ_2)ρ (au) plots for the studied complexes.
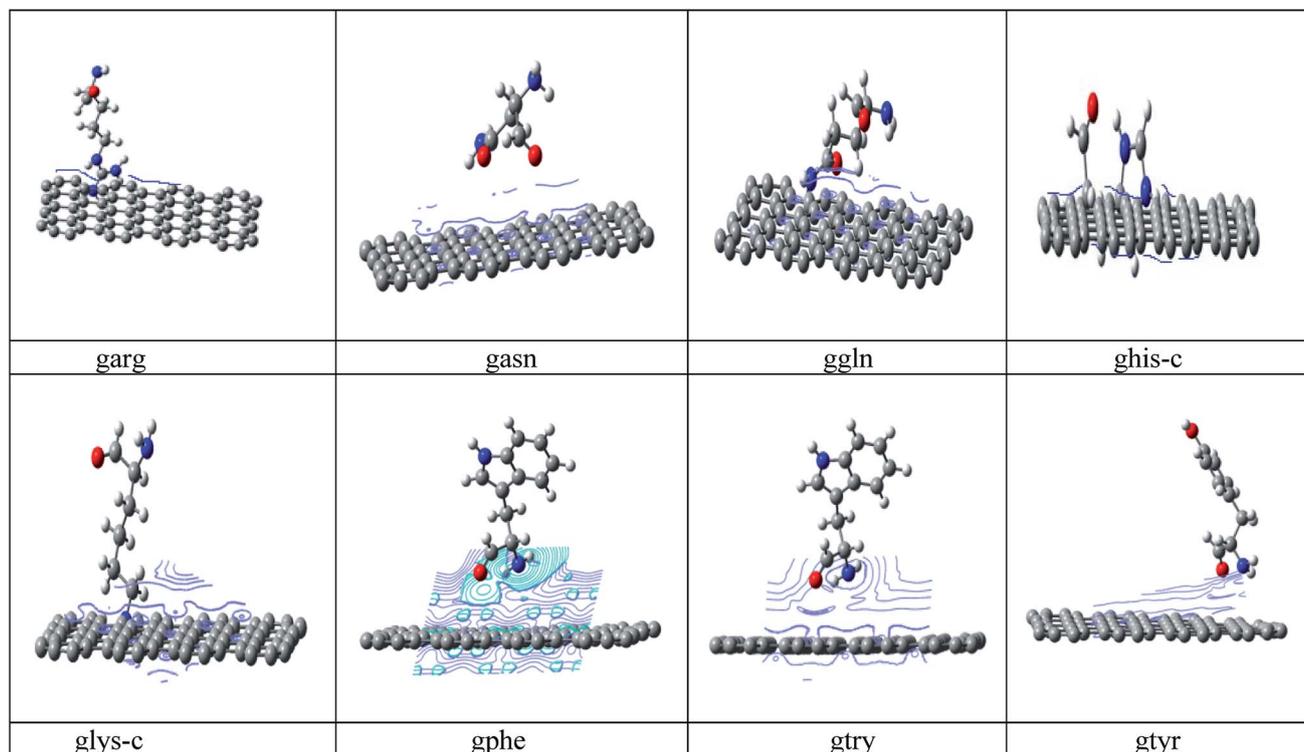
Fig. 4 Isosurface Plots of the studied graphene–peptide complexes. Gaussview has been used to generate these surfaces with isovalue = 0.0001.

complexes. The peaks are observed at both HOMO and LUMO level. PDOS analysis reflects the significant contribution from the p orbital contribution from carbon atom. The s orbital contribution from nitrogen and oxygen are less significant in these complexes.

3.3. AIM analysis and NCIPLOT analysis

The calculated electron density ρ_{BCP}, its Laplacian $\nabla^2 \rho_{BCP}$, total electron energy density H_{BCP}, and its components (the local kinetic energy density) G_{BCP}, and the local potential energy density V_{BCP} for grapheme–peptide complexes are reported in Table 3. The larger ρ value for these complexes indicated its strong interaction. The positive Laplacian H_{BCP} indicates a dominant closed shell (electrostatic) interaction. Hydrogen bond has increased the strength of these complexes. The nature of interactions is determined by the balance between the G_{BCP} and V_{BCP} values. If the absolute ratio of these quantities is less than 0.5, it is a shared interaction. For $0.5 < -G_{bcp}/V_{BCP} < 1$ values, the interaction is partly covalent in nature and for $-G_{bcp}/V_{BCP} > 1$, the interaction is noncovalent in nature. In our studied complexes, these interactions are noncovalent as the absolute values for $-G_{bcp}/V_{BCP} > 1$.[50]

NCI plots avoid complex algorithms and numerical pitfalls and offer valuable crystal bonding information, so the interactions have been studied by NCIPLOT graphs and isosurfaces. From NCIPLOT graphs, we plotted the reduced density gradient as a function of the density (mapped as isosurfaces) over the molecule of interest. The sign of the second Hessian eigen value

times the electron density (sign $(\lambda_2)\rho$) au help us to visualize the attractive/stabilizing (favourable) or repulsive (unfavourable) interactions. The second ingredient of the NCI index classifies the interactions as attractive or repulsive according to the sign of the second density Hessian eigen value (λ_2). NCI plot also allows an assessment of host–guest assembly complementarities and the extent to which weak interactions stabilize a complex along with the qualitative information regarding the involved molecular regions in the interaction. Red–blue–green colour scheme defines the nature of interactions. RDG (s) and electron density (ρ) combination allowed a rough partition of real space into bonding regions: high-s low-ρ corresponds to non-interacting density tails, low-s high-ρ to covalent bonds, and low-s low-ρ to noncovalent interactions. The value of sign(λ_2)ρ is color-mapped onto the s-isosurfaces. The favoured color scheme is a red-green-blue scale with red for ρ_{cut}^+ (repulsive) and blue for ρ_{cut}^- (attractive). We obtained the purple color for the studied complexes which is more inclined towards blue region. The electron density alone clearly distinguishes between the hydrogen bonds (the peak at sign(λ_2)$\rho \cong -0.05$ and the rest of the intermolecular interactions, represented by the wide band around zero density. The three-dimensional plot identifies the bonding regions corresponding to each of these peaks. The hydrogen bonds appear as round, much localized, blue NCI domains. The localized, high-density NCI regions for hydrogen-bonds indicate a relatively strong, highly-directional, intermolecular interaction while the weak interactions extend over large regions of intermolecular contacts. A cut-off value of s

Table 4 The absorption wavelength (nm) and oscillatory strength (f) of nanographene, peptides and graphene–peptide complexes in aqueous medium by TDDFT method

Complexes	λ_{abs} (nm)	f	Complexes	λ_{abs} (nm)	f
Graphene	660.53	0.2516	**garg**	989.92	0.0215
arg	230.39	0.0122	**gasn**	1076.07	0.0312
asn	137.07	0.1247	**ggln**	1192.24	0.0036
gln	149.44	0.0280	**ghis-c**	1012.02	0.0049
his-c	261.12	0.0727	**glys-c**	872.45	0.0021
lys-c	712.00	0.0963	**gphe**	1181.56	0.0049
phe	178.66	0.4773	**gtry**	1022.04	0.0046
try	194.82	0.6480	**gtyr**	1169.14	0.0042
tyr	181.16	0.5686			

close to zero, typically $s < 0.5$, is chosen in order to recover all the noncovalent interactions in the system, *i.e.* all the spikes of the 2D plots. The corresponding reduced density gradient isosurfaces give rise to closed domains in the molecular space which highlighted the spatial localization of the interactions within the system. See Fig. 3. The blue color of isosurface shows the existence of a strong electrostatic stabilizing contribution to the interaction. See Fig. 4. The hydrogen bonding interactions play a very important role in graphene–peptide complexes as the geometrical shape, stability and functionality of these functional materials depend on these noncovalent interactions.

3.4. Optical properties

In previous studies,[51,52] the absorption spectra and HOMO–LUMO (HL) gaps were analysed to study the correlation between the optical properties of graphene complexes, so TDDFT calculation has been carried out to study the optical properties of nanographene–peptide complexes in aqueous medium. Due to better optical properties of graphene, research interests have been shifted towards achieving improved photoresponse by using graphene as a supporting material. The electron mobility of graphene enables the photo-induced electron transfer in the interacting complex, which results in enhanced behaviour. The absorption wavelength of peptide complexes lies within (137–712 nm), but the absorption wavelength of studied graphene–peptide complexes lies >800 nm range. See Table 4. We find that HL gap of nanographene–peptide complexes are positively correlated to the wavelengths of the studied complexes.

Since the absorption wavelength of studied complexes does not lie in the visible region, we concluded that these complexes can find better application in biosensors rather than the fluorescent materials.

4. Conclusion

First principle calculations have been carried out to study the interactions, electronic and optical properties of eight graphene–peptide complexes. Results indicated strong bond interaction of **garg**, **ggln**, **glys-c** and **gphe** complexes. We have not observed any correlation between polarizability and bond

distance of the studied complexes as shown in a previous study in which polarizability of nucleobase molecules had determined their interaction strength with graphene/CNT.[33] Peptides have larger HL gap while nanographene–peptides have smaller HL gap, which showed strong interactions. PDOS figures show that the HOMO, LUMO of these complexes are solely from π electrons. AIM analysis and NCIPLOT results showed strong noncovalent interactions in the studied complexes. TDDFT calculations indicated the applicability of these complexes as biosensors. The absorption wavelength is positively correlated to the HL gap of the complexes. We believe that these studies will be useful for better understanding of peptide binding with planar carbon nanostructures, which has great implications toward developing biosensors. This interfacial graphene–biomolecules interaction permits peptides to exhibit excellent activity for nanobio-technological applications.

Conflicts of interest

There are no conflicts to declare.

Acknowledgements

References

1 (*a*) A. E. Rossini, F. Gala, M. Chinappi and G. Zollo, *Nanoscale*, 2018, **10**(13), 5928–5937; (*b*) Y. Y. Hu, S.-L. Sun, S. Muhammad, H.-L. Xu and Z.-M. Su, *J. Phys. Chem. C*, 2010, **114**(46), 19792–19798; (*c*) H. Chia, K. Muralia, T. D. Lia and S. Thomas, *Prog. Nat. Sci.: Mater. Int.*, 2019, **29**, 603–611.

2 (*a*) S. R. Russell and S. A. Claridge, *Anal. Bioanal. Chem.*, 2016, **408**, 2649–2658; (*b*) I. Saada and J. K. Pearson, *J. Mol. Struct.: THEOCHEM*, 2011, **969**, 76–82; (*c*) S. Banerjee and D. Bhattacharyya, *Comput. Mater. Sci.*, 2008, **44**(1), 41–45.

3 (*a*) C. Chung, Y. K. Kim, D. Shin, S. R. Ryoo, B. H. Hong and D. H. Min, *Acc. Chem. Res.*, 2013, **46**, 2211–2224; (*b*) b. J. Min, C.-W. Lee and H. K. Jeong, *J. Korean Phys. Soc.*, 2015, **67**, 507–511; (*c*) W. J. Jeong, J. Bu, L. J. Kubiatowicz, S. S. Chen, Y. Soo Kim and S. Hong, *Nano Convergence*, 2018, **5**, 38–46.

4 Y. Ohno, K. Maehashi and K. Matsumoto, *J. Am. Chem. Soc.*, 2010, **132**, 18012–18013.

5 M. Singh, M. Holzinger, M. Tabrizian, S. Winters, N. C. Berner, S. Cosnier and G. S. Duesberg, *J. Am. Chem. Soc.*, 2015, **137**, 2800–2803.

6 S. S. Chou, M. De, J. Y. Luo, V. M. Rotello, J. X. Huang and V. P. Dravid, *J. Am. Chem. Soc.*, 2012, **134**, 16725–16733.

7 Y. H. Ng, I. V. Lightcap, K. Goodwin, M. Matsumura and P. V. Kamat, *J. Phys. Chem. Lett.*, 2010, **1**, 2222–2227.

8 J. L. Vickery, A. J. Patil and S. Mann, *Adv. Mater.*, 2009, **21**, 2180–2184.

9 C. Berger, Z. Song, X. Li, X. Wu, N. Brown, C. Naud, D. Mayou, T. Li, J. Hass, A. N. Marchenkov, E. H. Conrad, P. N. First and W. A. de Heer, *Science*, 2006, **312**, 1191–1196.

10 J. B. Oostinga, H. B. Heersche, X. Liu, A. F. Morpurgo and L. M. K. Vandersypen, *Nat. Mater.*, 2008, **7**, 151–157.

11 P. Avouris, *Nano Lett.*, 2010, **10**, 4285–4294.

12 H. W. ang, Q. Hao, X. Yang, L. Lu and X. Wang, *Electrochem. Commun.*, 2009, **11**, 1158–1161.

13 C. L iu, Z. Yu, D. Neff, A. Zhamu and B. Z. Jang, *Nano Lett.*, 2010, **10**, 4863–4868.

14 R. Imran Jafri, N. Rajalakshmi and S. Ramaprabhu, *J. Mater. Chem.*, 2010, **20**, 7114.

15 L. Qu, Y. Liu, J. B. Baek and L. Dai, *ACS Nano*, 2010, **4**, 1321–1326.

16 X. Q. Zou, W. Shuai, J. Joshua, X. Minyu, W. Qiuming, C. L. Brooks III and C. Zhan, *J. Am. Chem. Soc.*, 2017, **139**, 1928–1936.

17 M. M. Flocco and S. L. J. Mowbray, *J. Mol. Biol.*, 1994, **235**, 709–717.

18 G. Duan, V. H. Smith and D. F. Weaver, *J. Phys. Chem. A*, 2000, **104**, 4521–4532.

19 G. Toth, C. R. Watts, R. F. Murphy and S. Lovas, *Proteins: Struct., Funct., Genet.*, 2001, **43**, 373–381.

20 G. B. McGaughey, M. Gagne and A. K. Rappe, *J. Biol. Chem.*, 1998, **273**, 15458–15463.

21 S. K. Burley and G. A. Petsko, *Science*, 1985, **229**, 23–28.

22 R. Bhattacharyya, R. P. Saha, U. Samanta and P. Chakrabarti, *J. Proteome Res.*, 2003, **2**, 255–263.

23 Z. E. Hughes and T. R. Walsh, *J. Mater. Chem. B*, 2015, **3**, 3211–3221.

24 R. B. Pandey, Z. F. Kuang, B. L. Farmer, S. S. Kim and R. R. Naik, *Soft Matter*, 2012, **8**, 9101–9109.

25 A. N. Camden, S. A. Barr and R. J. Berry, *J. Phys. Chem. B*, 2013, **117**, 10691–10697.

26 N. Dragneva, W. B. Floriano, D. Stauffer, R. C. Mawhinney, G. Fanchini and O. Rubel, *J. Chem. Phys.*, 2013, **139**, 174711.

27 C. M. Welch, A. N. Camden, S. A. Barr, G. M. Leuty, G. S. Kedziora and R. J. Berry, *J. Chem. Phys.*, 2015, **143**, 045104.

28 Y. C ui, S. N. Kim, S. E. Jones, L. L. Wissler, R. R. Naik and M. C. McAlpine, *Nano Lett.*, 2010, **10**, 4559–4565.

29 C.-H. Lu, J. Li, X. L. Zhang, A. X. Zheng, H. H. Yang, X. Chen and G. N. Chen, *Anal. Chem.*, 2011, **83**, 7276–7282.

30 S. K. B hunia and N. R. Jana, *ACS Appl. Mater. Interfaces*, 2011, **3**, 3335–3341.

31 S. N. K im, Z. Kuang, J. M. Slocik, S. E. Jones, Y. Cui, B. L. Farmer, M. C. McAlpine and R. R. Naik, *J. Am. Chem. Soc.*, 2011, **133**, 14480–14483.

32 L. O u, Y. Luo and G. Wei, *J. Phys. Chem. B*, 2011, **115**, 9813–9822.

33 C. Rajesh, C. Majumder, H. Mizuseki and Y. A. Kawazoe, *J. Chem. Phys.*, 2009, **130**, 124911.

34 M. J. Frisch, G. W. Trucks, H. B. Schlegel, G. E. Scuseria, M. A. Robb, J. R. Cheeseman, J. A. Montgomery Jr, T. Vreven, K. N. Kudin, J. C. Burant, J. M. Millam, S. S. Iyengar, J. Tomasi, V. Barone, B. Mennucci, M. Cossi, G. Scalmani, N. Rega, G. A. Petersson, H. Nakatsuji,

M. Hada, M. Ehara, K. Toyota, R. Fukuda, J. Hasegawa, M. Ishida, T. Nakajima, Y. Honda, O. Kitao, H. Nakai, M. Klene, X. Li, J. E. Knox, H. P. Hratchian, J. B. Cross, C. Adamo, J. Jaramillo, R. Gomperts, R. E. Stratmann, O. Yazyev, A. J. Austin, R. Cammi, C. Pomelli, W. J. Ochterski, P. Y. Ayala, K. Morokuma, G. A. Voth, P. Salvador, J. J. Dannenberg, V. G. Zakrzewski, S. Dapprich, A. D. Daniels, M. C. Strain, O. Farkas, K. D. Malick, D. A. Rabuck, K. Raghavachari, J. B. Foresman, J. V. Ortiz, Q. Cui, A. G. Baboul, S. Clifford, J. Cioslowski, B. B. Stefanov, G. Liu, A. Liashenko, P. Piskorz, I. Komaromi, R. L. Martin, D. J. Fox, T. Keith, M. A. Al-Laham, C. Y. Peng, A. Nanayakkara, M. Hallacombe, C. P. M. W. Gill, B. Johnson, W. Chen, M. W. Wong, C. Gonzalez and J. A. Pople, *J. A. C.02, Gaussian, Inc.*, Wallingford, CT, 2009.

35 (*a*) A. D. Becke, *J. Chem. Phys.*, 1993, **98**, 5648–5652; (*b*) C. Lee, W. Yang and R. G. Parr, *Phys. Rev. B: Condens. Matter Mater. Phys.*, 1988, **37**, 785–789; (*c*) Y. Zhao and D. G. Truhlar, *Theor. Chem. Acc.*, 2006, **120**(1–3), 215–241; (*d*) J. D. Chai and M. Head-Gordon, *Phys. Chem. Chem. Phys.*, 2008, **10**, 6615–6620.

36 M. D. Hanwell, D. E. Curtis, D. C. Lonie, T. Vandermeersch, E. Zurek and G. R. Hutchison, *J. Cheminf.*, 2012, **4**, 17.

37 R. Dennington, T. A. Keith and J. M. Millam, *GaussView, Version 6*, Semichem Inc., Shawnee Mission, KS, 2003.

38 J. Tomasi, B. Mennucci and R. Cammi, *Chem. Rev.*, 2005, **105**, 2999–3093.

39 M. Brandbyge, J. L. Mozos, P. Ordejón, J. Taylor and K. Stokbro, *Phys. Rev. B: Condens. Matter Mater. Phys.*, 2002, **65**(16), 165401.

40 M. Dion, H. Rydberg, E. Schröder, D. C. Langreth and B. L. Lundqvist, *Phys. Rev. Lett.*, 2004, **92**, 246401.

41 G. Kresse and J. Furthmüller, *Comput. Mater. Sci.*, 1996, **6**(1), 15–50.

42 P. L. A. Popelier, *Atoms in Molecules, An Introduction*, PrenticeHall, London, 2000, pp. 100–188.

43 U. Koch and P. L. A. Popelier, *J. Phys. Chem.*, 1995, **99**, 9747–9754.

44 J. R. Lane, J. Contreras-García, J. P. Piquemal, B. J. Miller and H. G. Kjaergaard, *J. Chem. Theory Comput.*, 2013, **9**, 3263–3266.

45 J. R. Lane, S. D. Schröder, G. C. Saunders and H. G. Kjaergaard, *J. Phys. Chem. A*, 2016, **120**, 6371–6378.

46 S. D. Schröder, J. H. Wallberg, J. A. Kroll, Z. Maroun, V. Vaida and H. G. Kjaergaard, *J. Phys. Chem. A*, 2015, **119**, 9692–9702.

47 C. L. Andersen, C. S. Jensen, K. Mackeprang, L. Du, S. Jørgensen and H. G. Kjaergaard, *J. Phys. Chem. A*, 2014, **118**, 11074–11082.

48 D. L. Thomsen, J. L. Axson, S. D. Schröder, J. R. Lane, V. Vaida and H. G. Kjaergaard, *J. Phys. Chem. A*, 2013, **117**, 10260–10273.

49 (*a*) R. A. Boto, F. Peccati, R. Laplaza, C. Quan, A. Carbone, J.-P. Piquemal, Y. Maday and J. Contreras-Garcia, *NCIPLOT4: A new step towards a fast quantification of noncovalent interactions*, 2010; (*b*) E. R. Johnson, S. Keinan, P. M. Sanchez, J. C. Garcia, A. J. Cohen and W. Yang, *J. Am.*

Chem. Soc., 2010, **132**, 6498–6506; (*c*) J. Contreras-Garcia, E. R. Johnson, S. Keinan, R. Chaudret, J.-P. Piquemal, D. N. Beratan and W. Yang, *J. Chem. Theory Comput.*, 2011, **7**, 625–632.

50 E. Espinosa, I. Alkorta, J. Elguero and E. Molins, *J. Chem. Phys.*, 2002, **117**, 5529–5542.

51 J. G. Feng, H. Z. Dong, L. Yu and L. Dong, *J. Mater. Chem. C*, 2017, **5**, 5984–5994.

52 J. G. Feng, H. Z. Dong, B. Pang, F. Shao, C. K. Zhang, L. Yu and L. Dong, *Phys. Chem. Chem. Phys.*, 2018, **20**, 15244–15253.